Quantum mechanical model for phonon excitation in electron diffraction and imaging using a Born-Oppenheimer approximation

B. D. Forbes,[1] A. V. Martin,[1,2] S. D. Findlay,[3] A. J. D'Alfonso,[1] and L. J. Allen[1]
[1]*School of Physics, University of Melbourne, Parkville, Victoria 3010, Australia*
[2]*Center for Free-Electron Laser Science, DESY, Hamburg 22607, Germany*
[3]*Institute of Engineering Innovation, School of Engineering, University of Tokyo, Tokyo 113-8656, Japan*
(Received 9 June 2010; published 3 September 2010)

We propose a many-body quantum-mechanical model for multiple thermal scattering of fast electrons due to phonon excitation in condensed matter. The key approximation upon which our approach is based is in the spirit of the Born-Oppenheimer approximation. We compare the conceptual underpinnings of this model to the well-known frozen phonon model for thermal scattering. Using our model it is possible to calculate the probability distribution of both elastically and inelastically scattered electrons. The model is also extended to encompass core-shell ionization.

DOI: 10.1103/PhysRevB.82.104103 PACS number(s): 61.05.jd

I. INTRODUCTION

A beam of fast electrons incident on a crystal produces a diffraction pattern which exhibits several well-known features including Bragg peaks, a diffuse background, higher-order Laue-zone (HOLZ) rings, and Kikuchi bands.[1] Phonon excitation (thermal scattering) makes an important contribution to many of these features, in particular, the diffuse background and Kickuchi lines.[2] Thermal scattering also makes the essential contribution to high-angle annular dark field measurements in scanning transmission electron microscopy.[3,4] It also plays an important role in transmission electron microscopy[5] and convergent-beam electron-diffraction patterns.[6,7]

The correct physics to model phonon excitation is based on many-body quantum mechanics, as expressed by the equations of Yoshioka,[8] by treating thermal scattering as a quantum excitation of the crystal. This theory has been used to model thermal scattering with both independent atomic vibrations[9] and with correlated atomic motion.[10] This framework has been successfully used to model ionization.[11] In this approach, one usually uses a single inelastic scattering approximation, appropriate for specimens considerably thinner than the mean free path for thermal scattering.

In this work, we use a many-body quantum-mechanical model and a Born-Oppenheimer-type approximation to derive a model for electron diffraction and imaging, including the contribution from thermally scattered electrons. Our model predicts the scattered intensity for a single electron, including multiple elastic and inelastic phonon scattering to all orders. This is an advantage over other approaches based on the Yoshioka formalism in which the single inelastic scattering approximation is usually made to allow for tractable calculations. In this model, we can explicitly calculate the elastic component and inelastic components of the scattered electron wave. The elastic waves from this model and an absorptive model derived from the Yoshioka formalism are compared and shown to agree well for both plane-wave and convergent-beam illumination. The model is extended to encompass core-shell ionization with a similar procedure to that in Ref. 12. However, here this is achieved through a natural generalization of the model presented, rather than the *ad hoc* approach in the earlier treatment.

In contrast to the fully quantum-mechanical approach used here, there is a widely used semiclassical approach to calculating thermal scattering, known as the frozen phonon model, which models elastic scattering from atoms displaced from their equilibrium positions.[6,7,13] It is motivated by the idea that the time taken for the fast electron to traverse the crystal is much faster than the oscillation period of an atom. Within this semiclassical model "the electron sees a snapshot of the atom frozen midvibration."[6] Each electron "sees" a different configuration, and the contributions of different electrons are summed incoherently in the detector plane. In practice this is implemented by a Monte Carlo integration. The frozen phonon model approach has been shown to agree well with an absorptive model of thermal scattering[14] and has produced simulations that compare well with experiment.[15] However, the frozen phonon model does not contain within its conceptual framework the momentum or energy transfer one would normally associate with inelastic scattering (in this case phonon excitation). This shortcoming has contributed to the mistaken assumption[16] that scattering from a moving lattice and the excitation of inelastic transitions are distinct effects. That this is not the case will be made clear by the model presented in this paper.

There have been notable investigations into why the frozen phonon model and rigorous quantum-mechanical models predict the same diffracted intensity. Wang[17] carried out a term-by-term comparison in series-expansion solutions of the frozen phonon model and the Yoshioka coupled channels equations (in density-matrix form).[8] More recently, Van Dyck[18] presented a simpler derivation of equivalence by separating the "elastic" (in the frozen phonon model the "time" or configuration independent part) and inelastic scattering intensities. It was shown that each model predicted the diffracted intensity with an equation of the same mathematical form for the single inelastic scattering case.

The model we present here provides a fresh perspective on why, at least from a numerical point of view, the semiclassical approach produces results which agree with experiment. Our model, based on many-body quantum mechanics,

leads to a scattering intensity which is numerically equivalent to that calculated using the frozen phonon model, albeit that the two models have quite different conceptual underpinnings.

II. FUNDAMENTAL EQUATIONS

Consider a fast electron incident on a crystalline specimen. The Schrödinger equation for the system can be written as

$$i\hbar\frac{\partial\Psi(\mathbf{r},\mathbf{r}_1,\ldots,\mathbf{r}_N,t)}{\partial t}=\left[-\frac{\hbar^2}{2m_e}\nabla_{\mathbf{r}}^2+H_c(\mathbf{r}_1,\ldots,\mathbf{r}_N)+H'(\mathbf{r},\mathbf{r}_1,\ldots,\mathbf{r}_N)\right]\Psi(\mathbf{r},\mathbf{r}_1,\ldots,\mathbf{r}_N,t), \tag{1}$$

where $\mathbf{r}$ is the coordinate of the incident electron and $\mathbf{r}_j$ the coordinate of the jth of N particles (nuclei or electrons) in the solid. The variable t denotes time. The term $(-\hbar^2/2m_e)\nabla_{\mathbf{r}}^2$ is the kinetic-energy operator for the fast electron and $H_c(\mathbf{r}_1,\ldots,\mathbf{r}_N)$ is the Hamiltonian for all the crystal particles. $H'(\mathbf{r},\mathbf{r}_1,\ldots,\mathbf{r}_N)$ describes the interaction of the incident electron with the crystal particles.

We simplify our notation and let $\boldsymbol{\tau}=\{\mathbf{r}_1,\ldots,\mathbf{r}_N\}$ be the set of all the position vectors which refer to particles in the crystal. We may then rewrite Eq. (1) as

$$i\hbar\frac{\partial\Psi(\mathbf{r},\boldsymbol{\tau},t)}{\partial t}=\left[-\frac{\hbar^2}{2m_e}\nabla_{\mathbf{r}}^2+H_c(\boldsymbol{\tau})+H'(\mathbf{r},\boldsymbol{\tau})\right]\Psi(\mathbf{r},\boldsymbol{\tau},t). \tag{2}$$

Since $H_c(\boldsymbol{\tau})$ and $H'(\mathbf{r},\boldsymbol{\tau})$ in Eq. (2) do not depend on time t, i.e., the crystal and the fast electron are isolated from the environment, we make the factorization $\Psi(\mathbf{r},\boldsymbol{\tau},t)\rightarrow\Psi(\mathbf{r},\boldsymbol{\tau})F(t)$. We can then write

$$\frac{i\hbar}{F(t)}\frac{\partial F(t)}{\partial t}=\frac{1}{\Psi(\mathbf{r},\boldsymbol{\tau})}\left[-\frac{\hbar^2}{2m_e}\nabla_{\mathbf{r}}^2+H_c(\boldsymbol{\tau})+H'(\mathbf{r},\boldsymbol{\tau})\right]\Psi(\mathbf{r},\boldsymbol{\tau})=E, \tag{3}$$

where the term before the first equality depends only on t, that after the first equality depends only on $\mathbf{r}$ and $\boldsymbol{\tau}$, and both these terms are thus equal to a constant E. It is easily verified that E has units of energy and it can be identified as the total energy of the system. So from Eq. (3) we obtain the time-independent Schrödinger equation

$$\left[-\frac{\hbar^2}{2m_e}\nabla_{\mathbf{r}}^2+H_c(\boldsymbol{\tau})+H'(\mathbf{r},\boldsymbol{\tau})\right]\Psi(\mathbf{r},\boldsymbol{\tau})=E\Psi(\mathbf{r},\boldsymbol{\tau}). \tag{4}$$

At this point $\Psi(\mathbf{r},\boldsymbol{\tau})$ can be expanded in terms of eigenfunctions of the crystal Hamiltonian $H_c(\boldsymbol{\tau})$

$$\Psi(\mathbf{r},\boldsymbol{\tau})=\sum_m\psi_m(\mathbf{r})a_m(\boldsymbol{\tau}), \tag{5}$$

where the normalized wave function $a_m(\boldsymbol{\tau})$ represents the mth stationary state of the crystal (of energy ε_m) and satisfies the equation

$$H_c(\boldsymbol{\tau})a_m(\boldsymbol{\tau})=\varepsilon_m a_m(\boldsymbol{\tau}). \tag{6}$$

One of the states $a_m(\boldsymbol{\tau})$ (not necessarily the ground state) is regarded as the initial state and is denoted by $a_0(\boldsymbol{\tau})$. Then $\psi_0(\mathbf{r})$ in Eq. (5) describes the fast electron after elastic scattering. Furthermore $\psi_m(\mathbf{r})$ $(m\neq 0)$ describes the fast electron after a transition in which the crystal is changed from $a_0(\boldsymbol{\tau})$ to $a_m(\boldsymbol{\tau})$. The energy of the electron in the state $\psi_0(\mathbf{r})$ is given by

$$E_0=E-\varepsilon_0. \tag{7}$$

For the case of inelastic scattering, the energy associated with $\psi_m(\mathbf{r})$, i.e., after the inelastic scattering event, is

$$E_m=E-\varepsilon_m\equiv\frac{h^2}{2m_e}k_m^2, \tag{8}$$

where k_m is the magnitude of the wave vector of the scattered electron. The energy loss of the incident fast electron after an inelastic scattering event which excites the crystal from the initial to the mth excited state is

$$E_{\text{loss}}=E_0-E_m=\varepsilon_m-\varepsilon_0. \tag{9}$$

The set of coordinates $\boldsymbol{\tau}$ can be partitioned into

$$\boldsymbol{\tau}_n=\{\text{the set of all the coordinates } \mathbf{r}_i \text{ which refer to nuclei}\}$$

and

$$\boldsymbol{\tau}_e=\{\text{the set of all the coordinates } \mathbf{r}_i \text{ which refer to electrons in the solid, relative to the coordinate of the appropriate nucleus}\}.$$

III. PHONON EXCITATION IN THE BORN-OPPENHEIMER APPROXIMATION

In this section, we will consider phonon excitation and assume that the wave functions for the crystal electrons are expressed in terms of the coordinates $\boldsymbol{\tau}_e$ relative to the appropriate nucleus. Hence, we employ the following factorization:

$$a_m(\boldsymbol{\tau})=b(\boldsymbol{\tau}_e)a_m(\boldsymbol{\tau}_n), \tag{10}$$

i.e., we assume that the nuclear and electronic subsystems are decoupled and that the electronic subsystem is not excited, which is consistent with how crystal wave functions are treated in previous models of phonon excitation.[9,10] If independent atomic vibrations are assumed, the nuclear wave functions $a_m(\boldsymbol{\tau}_n)$ are formed by describing each atom with a harmonic oscillator wave function.[9] If correlated atomic motion is modeled, each vibrational mode is described by a harmonic oscillator wave function.[10]

Substituting Eq. (10) into Eq. (5) gives

$$\Psi(\mathbf{r},\boldsymbol{\tau})=b(\boldsymbol{\tau}_e)\sum_m\psi_m(\mathbf{r})a_m(\boldsymbol{\tau}_n). \tag{11}$$

The crystal Hamiltonian in Eq. (6) is explicitly written as

$$H_c(\boldsymbol{\tau}) = -\frac{\hbar^2}{2m_e}\nabla^2_{\boldsymbol{\tau}_e} - \frac{\hbar^2}{2m_n}\nabla^2_{\boldsymbol{\tau}_n} + H'_c(\boldsymbol{\tau}), \tag{12}$$

where the first term is shorthand for a sum of kinetic-energy operators for the crystal electrons and the second for the nuclei with masses m_n (the generalization to nonmonatomic crystals is obvious).

The factorization in Eq. (10) is consistent with a model in which each nucleus is in an effective potential due to the interaction of neighboring atoms with that nucleus. This effective potential is given by the Coulomb interaction terms in $H'_c(\boldsymbol{\tau})$ involving nuclear coordinates, which will be labeled here as $H'^{(n)}_c(\boldsymbol{\tau}_n, \boldsymbol{\tau}_e)$. The remaining interaction terms depend only on the crystal electronic coordinates and will be labeled as $H'^{(ee)}_c(\boldsymbol{\tau}_e)$. The total energy of the system in this model is $E = E_0 + \epsilon_0^{(n)} + \epsilon_0^{(e)}$, where $\epsilon_0^{(n)}$ and $\epsilon_0^{(e)}$ are the nuclear and electronic energies, respectively.

We now propose the following ansatz for the wave function of the system:

$$\Psi(\mathbf{r}, \boldsymbol{\tau}) = b(\boldsymbol{\tau}_e)a(\boldsymbol{\tau}_n)\phi(\mathbf{r}, \boldsymbol{\tau}_n), \tag{13}$$

where $a(\boldsymbol{\tau}_n)$ is associated with the nuclear subsystem and $\phi(\mathbf{r}, \boldsymbol{\tau}_n)$ with the fast electron. Comparing Eq. (11) with Eq. (13), we see that the relationship between the functions in the ansatz and the energy eigenstates of the crystal is

$$a(\boldsymbol{\tau}_n)\phi(\mathbf{r}, \boldsymbol{\tau}_n) = \sum_m \psi_m(\mathbf{r})a_m(\boldsymbol{\tau}_n). \tag{14}$$

Such factorizations are clearly possible [trivially so if $a(\boldsymbol{\tau}_n)$ were to equal unity]. The key assumption we make is that $a(\boldsymbol{\tau}_n)$ might be chosen such that $\phi(\mathbf{r}, \boldsymbol{\tau}_n)$ satisfies

$$\nabla_{\boldsymbol{\tau}_n}\phi(\mathbf{r}, \boldsymbol{\tau}_n) \approx \mathbf{0}, \tag{15}$$

allowing us to neglect such derivatives of $\phi(\mathbf{r}, \boldsymbol{\tau}_n)$ in subsequent analysis. This assumption is akin to a Born-Oppenheimer approximation for the function $\phi(\mathbf{r}, \boldsymbol{\tau})$ associated with the fast electron, namely, that it is insensitive to *variations* in the coordinates of the crystal nuclei. This is consistent with the disparity in energy between the fast electron (hundreds of kiloelectronvolts) and the energy associated with the nuclei and phonon excitation (meV). On physical grounds we would expect the dominant term on the rhs of Eq. (14) to be $\psi_0(\mathbf{r})a_0(\boldsymbol{\tau}_n)$, where $a_0(\boldsymbol{\tau}_n)$ is the initial state of the crystal. This suggests that the choice $a(\boldsymbol{\tau}_n) = a_0(\boldsymbol{\tau}_n)$ in Eq. (14) would be a good one, a point we will return to in the discussion after Eq. (29).

Using Eqs. (13) and (15) in Eq. (4) we find

$$\begin{aligned} &-\frac{\hbar^2}{2m_e}a(\boldsymbol{\tau}_n)b(\boldsymbol{\tau}_e)\nabla^2_{\mathbf{r}}\phi(\mathbf{r}, \boldsymbol{\tau}_n) - \frac{\hbar^2}{2m_n}b(\boldsymbol{\tau}_e)\phi(\mathbf{r}, \boldsymbol{\tau}_n)\nabla^2_{\boldsymbol{\tau}_n}a(\boldsymbol{\tau}_n) \\ &\quad - \frac{\hbar^2}{2m_e}a(\boldsymbol{\tau}_n)\phi(\mathbf{r}, \boldsymbol{\tau}_n)\nabla^2_{\boldsymbol{\tau}_e}b(\boldsymbol{\tau}_e) + H'_c(\boldsymbol{\tau})a(\boldsymbol{\tau}_n)b(\boldsymbol{\tau}_e)\phi(\mathbf{r}, \boldsymbol{\tau}_n) \\ &\quad + H'(\mathbf{r}, \boldsymbol{\tau})a(\boldsymbol{\tau}_n)b(\boldsymbol{\tau}_e)\phi(\mathbf{r}, \boldsymbol{\tau}_n) \\ &\quad = Ea(\boldsymbol{\tau}_n)b(\boldsymbol{\tau}_e)\phi(\mathbf{r}, \boldsymbol{\tau}_n). \end{aligned} \tag{16}$$

Now we multiply Eq. (16) through by $b^*(\boldsymbol{\tau}_e)$ and integrate up over the electronic degrees of freedom to obtain

$$\begin{aligned} &-\frac{\hbar^2}{2m_e}a(\boldsymbol{\tau}_n)\nabla^2_{\mathbf{r}}\phi(\mathbf{r}, \boldsymbol{\tau}_n) - \frac{\hbar^2}{2m_n}\phi(\mathbf{r}, \boldsymbol{\tau}_n)\nabla^2_{\boldsymbol{\tau}_n}a(\boldsymbol{\tau}_n) + [(V_0^{(e)} + E_0^{(e)}) \\ &\quad + \tilde{H}'^{(n)}_c(\boldsymbol{\tau}_n) + \tilde{H}'(\mathbf{r}, \boldsymbol{\tau}_n)]a(\boldsymbol{\tau}_n)\phi(\mathbf{r}, \boldsymbol{\tau}_n) \\ &\quad = Ea(\boldsymbol{\tau}_n)\phi(\mathbf{r}, \boldsymbol{\tau}_n), \end{aligned} \tag{17}$$

where

$$V_0^{(e)} = \int b^*(\boldsymbol{\tau}_e)H'^{(ee)}_c(\boldsymbol{\tau}_e)b(\boldsymbol{\tau}_e)d\boldsymbol{\tau}_e, \tag{18}$$

$$E_0^{(e)} = \int b^*(\boldsymbol{\tau}_e)\left[-\frac{\hbar^2}{2m_e}\nabla^2_{\boldsymbol{\tau}_e}\right]b(\boldsymbol{\tau}_e)d\boldsymbol{\tau}_e, \tag{19}$$

$$\tilde{H}'^{(n)}_c(\boldsymbol{\tau}_n) = \int b^*(\boldsymbol{\tau}_e)H'^{(n)}_c(\boldsymbol{\tau}_e, \boldsymbol{\tau}_n)b(\boldsymbol{\tau}_e)d\boldsymbol{\tau}_e, \tag{20}$$

and

$$\tilde{H}'(\mathbf{r}, \boldsymbol{\tau}_n) = \int b^*(\boldsymbol{\tau}_e)H'(\mathbf{r}, \boldsymbol{\tau})b(\boldsymbol{\tau}_e)d\boldsymbol{\tau}_e. \tag{21}$$

Noting that $\epsilon_0^{(e)} = E_0^{(e)} + V_0^{(e)}$, we can cancel terms from each side of Eq. (17) and divide through by $a(\boldsymbol{\tau}_n)\phi(\mathbf{r}, \boldsymbol{\tau}_n)$ to find

$$\begin{aligned} &-\frac{\hbar^2}{2m_e}\frac{1}{\phi(\mathbf{r}, \boldsymbol{\tau}_n)}\nabla^2_{\mathbf{r}}\phi(\mathbf{r}, \boldsymbol{\tau}_n) - \frac{\hbar^2}{2m_n}\frac{1}{a(\boldsymbol{\tau}_n)}\nabla^2_{\boldsymbol{\tau}_n}a(\boldsymbol{\tau}_n) + \tilde{H}'^{(n)}_c(\boldsymbol{\tau}_n) \\ &\quad + \tilde{H}'(\mathbf{r}, \boldsymbol{\tau}_n) \\ &\quad = E_0 + \epsilon_0^{(n)}. \end{aligned} \tag{22}$$

For this equation to be valid for all $\mathbf{r}$ and $\boldsymbol{\tau}_n$, we must have that

$$-\frac{\hbar^2}{2m_e}\frac{1}{\phi(\mathbf{r}, \boldsymbol{\tau}_n)}\nabla^2_{\mathbf{r}}\phi(\mathbf{r}, \boldsymbol{\tau}_n) + \tilde{H}'(\mathbf{r}, \boldsymbol{\tau}_n) = E_0 + \epsilon_0^{(n)} - \epsilon(\boldsymbol{\tau}_n) \tag{23}$$

and

$$-\frac{\hbar^2}{2m_n}\frac{1}{a(\boldsymbol{\tau}_n)}\nabla^2_{\boldsymbol{\tau}_n}a(\boldsymbol{\tau}_n) + \tilde{H}'^{(n)}_c(\boldsymbol{\tau}_n) = \epsilon(\boldsymbol{\tau}_n), \tag{24}$$

where $\epsilon(\boldsymbol{\tau}_n)$ is a separation function.

Now consider the situation where the fast electron is far from the specimen, prior to incidence. The interaction Hamiltonian $\tilde{H}'(\mathbf{r}, \boldsymbol{\tau}_n)$ is negligible, and from Eq. (14) we have $\phi(\mathbf{r}, \boldsymbol{\tau}_n) = \psi_0(\mathbf{r})a_0(\boldsymbol{\tau}_n)/a(\boldsymbol{\tau}_n)$. Equation (23) becomes

$$-\frac{\hbar^2}{2m_e}\frac{1}{\psi_0(\mathbf{r})}\nabla^2_{\mathbf{r}}\psi_0(\mathbf{r}) = E_0 + \epsilon_0^{(n)} - \epsilon(\boldsymbol{\tau}_n). \tag{25}$$

The left-hand side of the above equation is the initial kinetic energy of the fast electron, which is precisely E_0. Therefore $\epsilon(\boldsymbol{\tau}_n) = \epsilon_0^{(n)}$, and we can write Eqs. (23) and (24) as

$$-\frac{\hbar^2}{2m_e}\nabla^2_{\mathbf{r}}\phi(\mathbf{r}, \boldsymbol{\tau}_n) + \tilde{H}'(\mathbf{r}, \boldsymbol{\tau}_n)\phi(\mathbf{r}, \boldsymbol{\tau}_n) = E_0\phi(\mathbf{r}, \boldsymbol{\tau}_n) \tag{26}$$

and

$$-\frac{\hbar^2}{2m_n}\nabla^2_{\boldsymbol{\tau}_n} a(\boldsymbol{\tau}_n) + \tilde{H}'^{(n)}_c(\boldsymbol{\tau}_n) a(\boldsymbol{\tau}_n) = \epsilon^{(n)}_0 a(\boldsymbol{\tau}_n). \tag{27}$$

Equation (26) can be solved using the multislice method[13] for a set of nuclear coordinates $\boldsymbol{\tau}_n$.

From Eq. (11) we obtain the following boundary condition at the entrance surface:

$$\Psi(\mathbf{r}_\perp, z=0, \boldsymbol{\tau}) = b(\boldsymbol{\tau}_e) a_0(\boldsymbol{\tau}_n) \psi_0(\mathbf{r}_\perp, z=0), \tag{28}$$

where we have decomposed $\mathbf{r}$ into a component $\mathbf{r}_\perp$ parallel to the entrance surface and a perpendicular component z. Using Eq. (13) this leads to

$$\phi(\mathbf{r}_\perp, z=0, \boldsymbol{\tau}_n) = \frac{a_0(\boldsymbol{\tau}_n)}{a(\boldsymbol{\tau}_n)} \psi_0(\mathbf{r}_\perp, z=0), \tag{29}$$

which is used when solving Eq. (26). Zeroes in $a(\boldsymbol{\tau}_n)$ do not present a problem since at those zeroes $\Psi(\mathbf{r}_\perp, z=0, \boldsymbol{\tau})$ would also be zero [see Eq. (13)] and thus we would not need to evaluate Eq. (26).

We note that Eq. (27) is Eq. (6) restricted to the phonon subsector of the inelastic scattering. Furthermore, the initial state of the nuclear subsystem $a_0(\boldsymbol{\tau}_n)$ satisfies Eq. (27) exactly. At nonzero temperatures, a typical energy level will be highly degenerate, so there may be many other crystal eigenstates $a_n(\boldsymbol{\tau}_n)$ which also satisfy Eq. (27). We argue, by looking at the boundary conditions, that the error in Eq. (15) is minimized by the choice $a(\boldsymbol{\tau}_n)=a_0(\boldsymbol{\tau}_n)$. Substituting Eq. (29) into Eq. (15), we see that the choice $a(\boldsymbol{\tau}_n)=a_0(\boldsymbol{\tau}_n)$ gives no error at the entrance surface whereas other choices for $a(\boldsymbol{\tau}_n)$ result in a nonzero error. Close to the entrance surface where $\psi_0(\mathbf{r})$ remains dominant, the error will still be minimized for the choice $a(\boldsymbol{\tau}_n)=a_0(\boldsymbol{\tau}_n)$. Since we will use the multislice method to solve for $\phi(\mathbf{r}, \boldsymbol{\tau}_n)$, any errors near the entrance surface will propagate through the crystal to the exit surface. Therefore we will proceed with the choice of $a(\boldsymbol{\tau}_n)=a_0(\boldsymbol{\tau}_n)$.

The probability distribution of the fast electron is modeled by the quantum-mechanical average over nuclear coordinates

$$\begin{aligned} I(\mathbf{r}) \equiv I(\mathbf{r}_\perp, z) &= \int |\Psi(\mathbf{r}_\perp, z, \boldsymbol{\tau})|^2 d\boldsymbol{\tau} \\ &= \int |\phi(\mathbf{r}_\perp, z, \boldsymbol{\tau}_n)|^2 |a_0(\boldsymbol{\tau}_n)|^2 d\boldsymbol{\tau}_n \int |b(\boldsymbol{\tau}_e)|^2 d\boldsymbol{\tau}_e \\ &= \int |\phi(\mathbf{r}_\perp, z, \boldsymbol{\tau}_n)|^2 |a_0(\boldsymbol{\tau}_n)|^2 d\boldsymbol{\tau}_n. \end{aligned} \tag{30}$$

This integral can be solved via Monte Carlo calculation, where $|a_0(\boldsymbol{\tau}_n)|^2$ is acting as a probability distribution, and where the $\phi(\mathbf{r}_\perp, z, \boldsymbol{\tau}_n)$ are obtained via the multislice method.

Equation (30) gives the probability distribution for a single electron. In practice, an experimental image is built up from many electrons. While it was reasonable to assume that for a single electron, the system was not influenced by the environment and thus the crystal was initially in an energy eigenstate, for subsequent electrons thermal contact with the environment must be taken into account. Electrons incident at different times during a measurement scatter from different initial crystal states, chosen from a thermal statistical ensemble. A measurement is modeled as the incoherent sum of electrons that have scattered from different initial states and is written

$$\begin{aligned} I(\mathbf{r}_\perp, z) &= \sum_i I_i(\mathbf{r}_\perp, z) \\ &= \sum_i \int |\Psi_i(\mathbf{r}_\perp, z, \boldsymbol{\tau})|^2 d\boldsymbol{\tau} \\ &= \sum_i \int |\phi(\mathbf{r}_\perp, z, \boldsymbol{\tau}_n)|^2 |a_i(\boldsymbol{\tau}_n)|^2 d\boldsymbol{\tau}_n \int |b(\boldsymbol{\tau}_e)|^2 d\boldsymbol{\tau}_e \\ &= \int |\phi(\mathbf{r}_\perp, z, \boldsymbol{\tau}_n)|^2 \left\{ \sum_i |a_i(\boldsymbol{\tau}_n)|^2 \right\} d\boldsymbol{\tau}_n \\ &\equiv \int |\phi(\mathbf{r}_\perp, z, \boldsymbol{\tau}_n)|^2 P(\boldsymbol{\tau}_n) d\boldsymbol{\tau}_n. \end{aligned} \tag{31}$$

This average over initial states was not considered explicitly in the recent Van Dyck paper[18] though it had been considered in detail earlier by Van Dyck and co-workers.[19,20]

If the crystal is modeled as a set of independent harmonic oscillators, then the ith atom will have the following probability distribution:

$$P(\boldsymbol{\tau}^i_n) = \sqrt{\frac{1}{2\pi\langle (u^i)^2 \rangle}} \exp[(\boldsymbol{\tau}^i_n - \boldsymbol{R}^i)^2 / \langle (u^i)^2 \rangle], \tag{32}$$

where $\boldsymbol{R}^i$ is the equilibrium position of the atom and $\langle (u^i)^2 \rangle$ is the mean-squared displacement of the atom. Experimental and simulated values for the mean-square displacement, or the closely related Debye-Waller factor, are available in the literature.[21,22]

It is important to note that $I(\mathbf{r})$ contains contributions from elastic scattering and thermal inelastic scattering to all orders, as indicated by Eq. (14). This is an advantage over absorptive quantum-mechanical models[23] which make, in the usual implementation, a single inelastic scattering approximation and gives correspondingly better agreement with experiment for thicker specimens.[15]

Solving Eq. (31) using the Monte Carlo method, with the distribution taken as Eq. (32), is numerically equivalent to the frozen phonon model.[6] However, the interpretation and conceptual basis underlying the theory presented here is very different to that of the frozen phonon model. Our model requires Eq. (26) to be calculated for multiple atomic configurations in order to model the scattering of a single electron. In contrast, the frozen-phonon model proposes that each electron scatters from only a single atomic configuration. It should also be noted that we solve for a *wave function* with parametric nuclear coordinate dependence whereas the frozen phonon model explicitly considers the incoherent sum of *intensities*. Furthermore, our formalism provides an explicit mathematical description of the approximations and errors associated with this calculation, which is not provided by the frozen phonon model.

IV. WAVE FUNCTIONS

An additional advantage of the model presented here is that it can be used to calculate the elastic and inelastic scattered waves $\psi_m(\mathbf{r})$ using

$$\psi_m(\mathbf{r}) = \int_V a_m^*(\boldsymbol{\tau}_n) a(\boldsymbol{\tau}_n) \phi(\mathbf{r}, \boldsymbol{\tau}_n) d\boldsymbol{\tau}_n, \tag{33}$$

which follows directly from Eq. (14). The elastic wave is obtained for $m=0$. The integration in Eq. (33) can be calculated in the same manner as Eq. (31), the key difference being that Eq. (33) involves a coherent summation of $\phi(\mathbf{r}, \boldsymbol{\tau}_n)$.

It must be emphasized that the definition and construction of elastic and inelastic waves is only rigorously possible here if we assume a certain initial state for the crystal; the coherent average over $\boldsymbol{\tau}_n$ in Eq. (33) does not include a thermal average over the possible initial states of the crystal. Nevertheless, it is interesting to consider Eq. (33) for the "ground state," where we include a coherent average over initial states

$$\overline{\psi_0}(\mathbf{r}) = \sum_i \int_V |a_i(\boldsymbol{\tau}_n)|^2 \phi(\mathbf{r}, \boldsymbol{\tau}_n) d\boldsymbol{\tau}_n = \int_V \phi(\mathbf{r}, \boldsymbol{\tau}_n) P(\boldsymbol{\tau}_n) d\boldsymbol{\tau}_n. \tag{34}$$

This might loosely be thought of as an average elastic wave function over the range of possible initial thermal states. As we show below, this result is numerically equivalent to the elastic wave function calculated in the absorptive model assuming a Debye-Waller factor smeared potential. It is also what would be obtained experimentally in an off-axis holographic reconstruction of the elastic wave, as shown recently by Rother *et al.*[16]

To illustrate this, the elastic wave function, given by Eq. (34) was calculated using standard multislice code to implement the Monte Carlo integration method. The $\phi(\mathbf{r}, \boldsymbol{\tau}_n)$ were calculated using Eq. (26) for a configuration $\boldsymbol{\tau}_n$ picked from the distribution given by Eq. (32). The exit surface wave functions from each pass were summed coherently. Simulations shown in Fig. 1 were performed with plane-wave illumination for samples of $SrTiO_3$ with thicknesses 20, 200, and 1000 Å, and with a supercell tiling of 5×5 unit cells. Figures 1(a) and 1(b) show an excellent agreement between the elastic wave function predicted by our model and the standard absorptive model simulation[23] for the crystal thicknesses of 20 and 200 Å. This suggests that the exit surface wave function calculated with Eq. (34) is equivalent to the usual elastic calculation using a Debye-Waller factor smeared elastic potential and including absorption. It also suggests that the approximation made in Eq. (15) is valid. At a crystal thickness of 1000 Å, shown in Fig. 1(c), there is also a very favorable agreement, except for a small discrepancy in the peak height. This could be due to errors in our model from the approximation made in Eq. (15).

Using our model, diffraction patterns were calculated. The diffraction pattern for a 200-Å-thick crystal of $SrTiO_3$ with

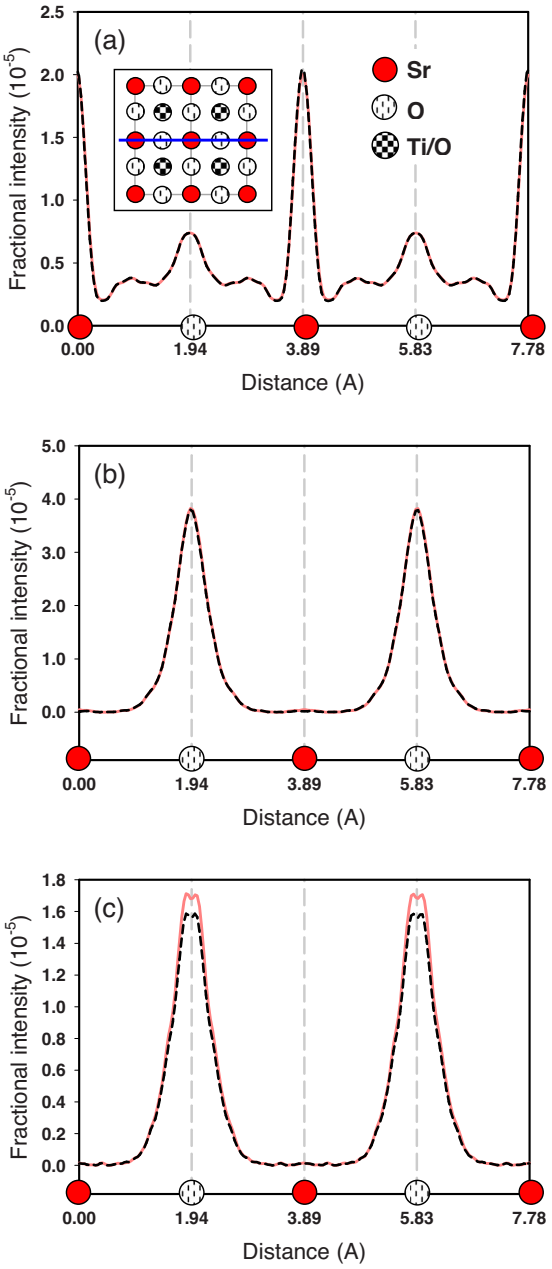

FIG. 1. (Color online) Elastic exit surface intensity $|\overline{\psi_0}|^2$ with plane-wave illumination, constructed by coherent summation using Eq. (34) for (a) a 20-Å-thick specimen of $SrTiO_3$ along the line scan indicated in the inset. Part (b) is a similar result for a 200-Å-thick specimen and (c) that for a 1000 Å specimen. The red (solid) lines represent the results of our model and the black (dashed) lines represent data from an absorptive model calculation.

plane-wave illumination is shown in Fig. 2(a) and one can clearly see the Bragg spots and HOLZ ring superimposed on the diffuse background. The diffraction patterns are displayed on a log scale[6]

$$I'(\mathbf{k}) = \ln[1 + CI(\mathbf{k})/I_{\max}], \tag{35}$$

where C is appropriately chosen to bring out the important features. The diffraction pattern due to elastically scattered

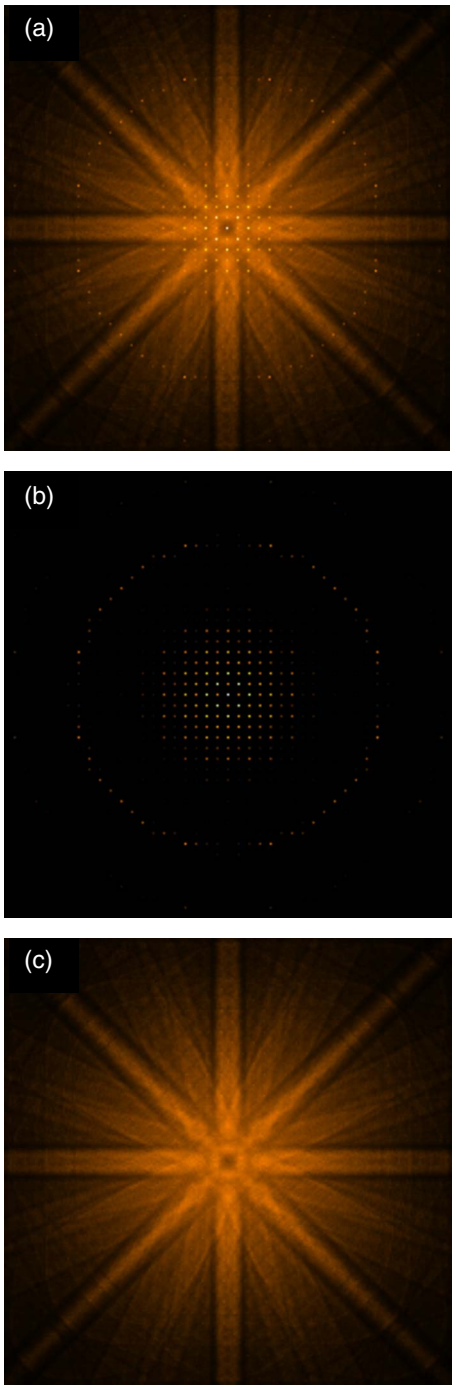

FIG. 2. (Color online) Diffraction pattern components for a 200-Å-thick $SrTiO_3$ specimen formed under plane-wave illumination displayed with a log scaling factor C of 1.5×10^5 in Eq. (35); (a) the full intensity, (b) elastically electrons only, and (c) inelastically (thermally) scattered electrons only.

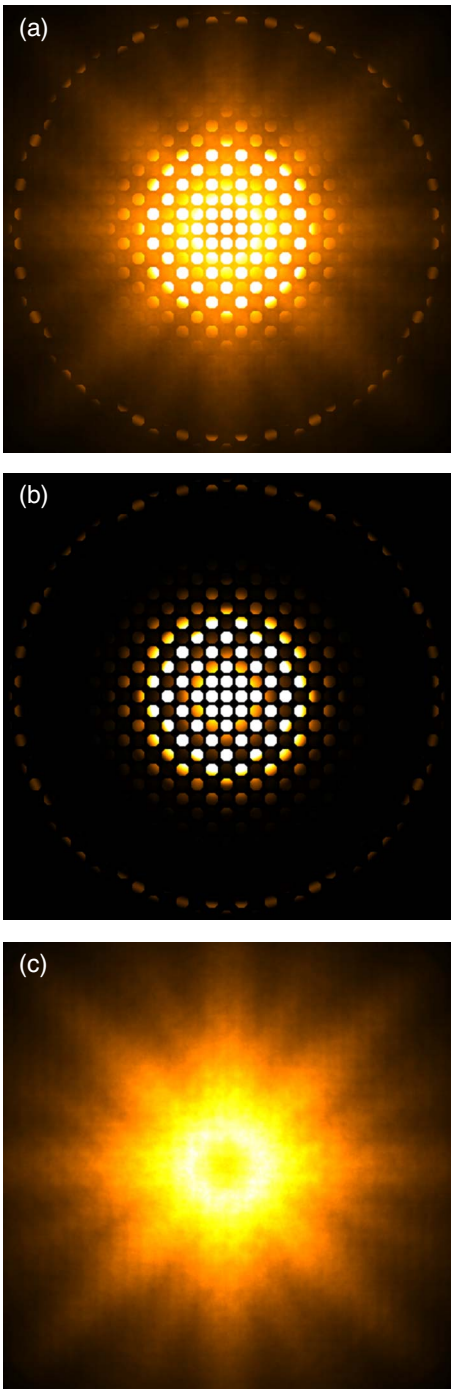

FIG. 3. (Color online) Diffraction pattern components for a 60-Å-thick $SrTiO_3$ specimen formed with a convergent probe of aperture 0.112 $Å^{-1}$ positioned over a Sr column and displayed with a log scaling factor C of 1.5×10^5 in Eq. (35); (a) the full intensity, (b) elastically electrons only, and (c) inelastically (thermally) scattered electrons only.

electrons, calculated using Eq. (34), is shown in Fig. 2(b). It contains Bragg peaks and the HOLZ ring but no diffuse background. Subtracting the elastic contribution (b) from the total diffraction pattern (a) removes precisely the Bragg peaks and HOLZ ring, leaving only the diffuse background of inelastically scattered electrons, as shown in Fig. 2(c).

A convergent beam electron-diffraction simulation is shown in Fig. 3 for a specimen of $SrTiO_3$, 60 Å thick with a probe-forming aperture of 0.112 $Å^{-1}$ (chosen so that the diffraction disks just do not overlap), no aberrations or defocus, and the probe positioned on a strontium column. As for plane-wave illumination, we see the partitioning between elastic and inelastic features in Figs. 3(b) and 3(c).

V. INCORPORATING IONIZATION

In this section, we extend the model presented earlier to account for core-shell ionization. Phonon excitation is still included by leaving in the nuclear coordinates $\boldsymbol{\tau}_n$, to be integrated over later in a Monte Carlo procedure, as before. The ionization is treated using the transition potentials H_{n0} which arise in the Yoshioka formalism.[8] We generalize the ansatz given by Eq. (13) to allow for electronic excitation as follows:

$$\Psi(\mathbf{r},\boldsymbol{\tau}) = a(\boldsymbol{\tau}_n)\sum_m b_m(\boldsymbol{\tau}_e)\phi_m(\mathbf{r},\boldsymbol{\tau}_n), \tag{36}$$

where m indicates the level of excitation of the ionized crystal. The wave functions $b_m(\boldsymbol{\tau}_e)$ are a set of orthogonal basis functions. Since we have assumed that the nuclear and electronic motions are decoupled, ionization only affects functions which depend on the coordinates $\boldsymbol{\tau}_e$ or $\mathbf{r}$. Each of the functions $\phi_m(\mathbf{r},\boldsymbol{\tau}_n)$ satisfies the Born-Oppenheimer approximation in Eq. (15).

We now follow the derivation in Sec. III. Instead of multiplying through by $b^*(\boldsymbol{\tau}_e)$, as we did in Eq. (17), we now will multiply through by $b_l^*(\boldsymbol{\tau}_e)$ to pick out the lth ionization state. We arrive at an analog of Eq. (26), which for clarity we separate into two equations

$$\begin{aligned} &-\frac{\hbar^2}{2m_e}\nabla_{\mathbf{r}}^2\phi_0(\mathbf{r},\boldsymbol{\tau}_n) + \tilde{H}'_{00}(\mathbf{r},\boldsymbol{\tau}_n)\phi_0(\mathbf{r},\boldsymbol{\tau}_n) \\ &\quad + \sum_{m\neq 0}\tilde{H}'_{0m}(\mathbf{r},\boldsymbol{\tau}_n)\phi_m(\mathbf{r},\boldsymbol{\tau}_n) \\ &\quad = E_0\phi_0(\mathbf{r},\boldsymbol{\tau}_n) \end{aligned} \tag{37}$$

and

$$\begin{aligned} &-\frac{\hbar^2}{2m_e}\nabla_{\mathbf{r}}^2\phi_l(\mathbf{r},\boldsymbol{\tau}_n) + \tilde{H}'_{ll}(\mathbf{r},\boldsymbol{\tau}_n)\phi_l(\mathbf{r},\boldsymbol{\tau}_n) + \tilde{H}'_{l0}(\mathbf{r},\boldsymbol{\tau}_n)\phi_0(\mathbf{r},\boldsymbol{\tau}_n) \\ &\quad = E_l\phi_l(\mathbf{r},\boldsymbol{\tau}_n), \end{aligned} \tag{38}$$

where E_l is the energy of the fast electron after the ionization event l, and

$$\tilde{H}'_{lm}(\mathbf{r},\boldsymbol{\tau}_n) = \int b_l^*(\boldsymbol{\tau}_e)H'(\mathbf{r},\boldsymbol{\tau})b_m(\boldsymbol{\tau}_e)d\boldsymbol{\tau}_e. \tag{39}$$

In Eq. (38) we have made the approximation $\tilde{H}'_{lm}(\mathbf{r},\boldsymbol{\tau}_n)\approx 0$ for $l,m\neq 0$, which corresponds to assuming that the fast electron is likely to find the target electron in the ground state. In practice it is also a good approximation to replace $\tilde{H}'_{ll}(\mathbf{r},\boldsymbol{\tau}_n)$ with $\tilde{H}'_{00}(\mathbf{r},\boldsymbol{\tau}_n)$.

Following Coene and Van Dyck,[24] we can start from Eq. (38) and arrive at

$$\phi_l(\mathbf{r}_\perp,z',\boldsymbol{\tau}_n) \approx -\frac{2m_e}{\hbar^2}\frac{i}{4\pi k_l}\tilde{H}_{l0}\phi_0(\mathbf{r}_\perp,z',\boldsymbol{\tau}_n), \tag{40}$$

where z' is the depth at which ionization occurs and $k_l^2 = (2m/h^2)E_l$. This allows us to rewrite Eq. (37) as

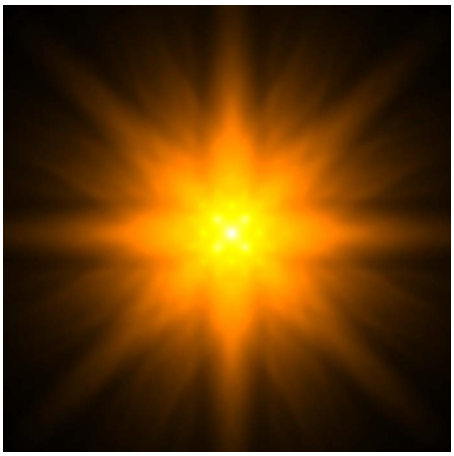

FIG. 4. (Color online) Simulation of an energy-spectroscopic diffraction pattern for electrons that have ionized an oxygen K-shell electron for plane-wave illumination in $SrTiO_3$. The energy filter is set at 1 eV above threshold. The sample was 200 Å thick with a tiling of 8×8 unit cells.

$$\begin{aligned} &\left[-\frac{\hbar^2}{2m_e}\nabla_{\mathbf{r}}^2 + \tilde{H}'_{00}(\mathbf{r},\boldsymbol{\tau}_n)\right. \\ &\qquad \left. -\frac{2m_e}{\hbar^2}\frac{i}{4\pi}\sum_m\frac{1}{k_m}\tilde{H}'_{0m}(\mathbf{r},\boldsymbol{\tau}_n)\tilde{H}'_{m0}(\mathbf{r},\boldsymbol{\tau}_n)\right]\phi_0(\mathbf{r},\boldsymbol{\tau}_n) \\ &\quad = E_0\phi_0(\mathbf{r},\boldsymbol{\tau}_n). \end{aligned} \tag{41}$$

The previous equation can be solved using the multislice method. In practice, the absorption from the elastic channel due to ionization, represented by the term $\Sigma_m\tilde{H}'_{0m}(\mathbf{r},\boldsymbol{\tau}_n)\tilde{H}'_{m0}(\mathbf{r},\boldsymbol{\tau}_n)/k_m$, is minimal and can be neglected, in which case Eq. (41) reduces to Eq. (26).

The signal in the diffraction plane from electrons that have induced ionization is

$$I_{\text{ion}}(\mathbf{q}_\perp) = \sum_{l\neq 0}\int |\phi_l(\mathbf{q}_\perp,d,\boldsymbol{\tau}_n)|^2|a(\boldsymbol{\tau}_n)|^2 d\boldsymbol{\tau}_n, \tag{42}$$

where d is the thickness of the specimen, and in practice the sum over l would be restricted those transitions which make a significant contribution to the total signal.

The procedure for calculating the signal due to ionization event l can be summarized as follows. (1) Pick a configuration $\boldsymbol{\tau}_n$ from the probability distribution $|a(\boldsymbol{\tau}_n)|^2$. (2) Calculate $\phi_0(\mathbf{r}_\perp,z',\boldsymbol{\tau}_n)$ using Eq. (41). (3) Calculate $\phi_l(\mathbf{r}_\perp,z',\boldsymbol{\tau}_n)$ using Eq. (40). (4) Propagate $\phi_l(\mathbf{r}_\perp,z',\boldsymbol{\tau}_n)$ to the exit surface using Eq. (38). Note that at this stage we can neglect the term $\tilde{H}'_{l0}(\mathbf{r},\boldsymbol{\tau}_n)\phi_0(\mathbf{r},\boldsymbol{\tau}_n)$ since the ionization event l has already occurred, and thus $\tilde{H}'_{l0}(\mathbf{r},\boldsymbol{\tau}_n)$ is zero in the subsequent region of the specimen. (5) Repeat for as many configurations $\boldsymbol{\tau}_n$ as needed for convergence.

In Fig. 4 we illustrate the results of the above procedure for electrons that have ionized an electron in the oxygen K shell for a $SrTiO_3$ crystal illuminated by a plane wave. In the diffraction pattern shown, the energy filter is set at 1 eV

above threshold. The sample was chosen to be 200 Å thick with a tiling of 8×8 unit cells. An approach similar to this has been employed by Dwyer.[25]

VI. CONCLUSION

We have presented a model for phonon excitation (thermal scattering) of a fast electron from a crystal. The key approximation behind the model is similar to the Born-Oppenheimer approximation used in molecular physics. We have compared this model to the well-known frozen phonon model, and although the frozen phonon model gives numerically equivalent results, the quantum-mechanical concepts used in this paper are strongly at variance with the semiclassical arguments used in the frozen phonon model. Here phonon excitation is considered as one of the inelastic scattering processes—physically a more natural view than "elastic scattering from a distorted lattice." The Born-Oppenheimer model we present is no more computationally demanding than the frozen phonon model and we are able to separate out the electrons which have scattered elastically and those which have excited a phonon. Lastly, we have extended this model to incorporate core-shell ionization.

ACKNOWLEDGMENTS

L.J.A. acknowledges support by the Australian Research Council. The authors acknowledge helpful dialog with Chris Witte.

[1] D. B. Williams and C. B. Carter, *Transmission Electron Microscopy* (Plenum Press, New York, 1996).
[2] C. R. Hall and P. B. Hirsch, Proc. R. Soc. London **286**, 158 (1965).
[3] A. Howie, J. Microsc. **117**, 11 (1979).
[4] S. J. Pennycook and D. E. Jesson, Ultramicroscopy **37**, 14 (1991).
[5] C. B. Boothroyd and R. E. Dunin-Borkowski, Ultramicroscopy **98**, 115 (2004).
[6] R. F. Loane, P. Xu, and J. Silcox, Acta Crystallogr., Sect. A: Found. Crystallogr. **47**, 267 (1991).
[7] D. A. Muller, B. Edwards, E. J. Kirkland, and J. Silcox, Ultramicroscopy **86**, 371 (2001).
[8] H. Yoshioka, J. Phys. Soc. Jpn. **12**, 618 (1957).
[9] A. Weickenmeier and H. Kohl, Acta Crystallogr., Sect. A: Found. Crystallogr. **54**, 283 (1998).
[10] A. V. Martin, S. D. Findlay, and L. J. Allen, Phys. Rev. B **80**, 024308 (2009).
[11] L. J. Allen and T. W. Josefsson, Phys. Rev. B **52**, 3184 (1995).
[12] S. D. Findlay, M. P. Oxley, S. J. Pennycook, and L. J. Allen, Ultramicroscopy **104**, 126 (2005).
[13] E. J. Kirkland, *Advanced Computing in Electron Microscopy* (Plenum Press, New York, 1998).
[14] S. D. Findlay, L. J. Allen, M. P. Oxley, and C. J. Rossouw, Ultramicroscopy **96**, 65 (2003).
[15] J. M. LeBeau, S. D. Findlay, L. J. Allen, and S. Stemmer, Phys. Rev. Lett. **100**, 206101 (2008).
[16] A. Rother, T. Gemming, and H. Lichte, Ultramicroscopy **109**, 139 (2009).
[17] Z. L. Wang, Acta Crystallogr., Sect. A: Found. Crystallogr. **54**, 460 (1998).
[18] D. Van Dyck, Ultramicroscopy **109**, 677 (2009).
[19] C. Fanidis, D. Van Dyck, and J. Van Landuyt, Ultramicroscopy **41**, 55 (1992).
[20] C. Fanidis, D. Van Dyck, and J. Van Landuyt, Ultramicroscopy **48**, 133 (1993).
[21] J. S. Reid, Acta Crystallogr., Sect. A: Found. Crystallogr. **39**, 1 (1983).
[22] H. X. Gao and L. M. Peng, Acta Crystallogr., Sect. A: Found. Crystallogr. **55**, 926 (1999).
[23] L. J. Allen, S. D. Findlay, M. P. Oxley, and C. J. Rossouw, Ultramicroscopy **96**, 47 (2003).
[24] W. Coene and D. Van Dyck, Ultramicroscopy **33**, 261 (1990).
[25] C. Dwyer and J. S. Barnard, Phys. Rev. B **74**, 064106 (2006).